Geomechanics and Engineering, *Vol. 33, No. 4 (2023) 393-400*
https://doi.org/10.12989/gae.2023.33.4.393

Study on fracture mechanics of granite specimens with different precast notch depths based on DIC method

Shuwen Cao* and Hao Shu[a]

School of Science, Xi'an University of Architecture and Technology, No.13 Yanta Road, Xi'an, Shannxi, 710055, P.R. China

(*Received October 10, 2022, Revised March 20, 2023, Accepted March 22, 2023*)

Abstract. Displacements near crack and stress intensity factor (SIF) are key parameters to solve rock failure issue when using fracture mechanics. In order to study the horizontal displacement and stress intensity factor of the mode I fracture, a series of three-point bending tests of granite specimens with central notch were carried out. The evolution of horizontal displacements of precast notch and crack tip opening displacements (CTOD) were analyzed based on the digital image correlation (DIC) method. Stress intensity factors for three-point bending beams with arbitrary span-to-width ratios(S/W) were calculated by using the WU-Carlsson analytical weight function for edge-crack finite width plate and the analytical solution of un-cracked stress by Filon. The present study provides a high efficient and accurate method for fracture mechanics analysis of the three-point bending granite beams.

Keywords: digital image correlation; horizontal displacements; three-point bending; stress intensity factor; weight

1. Introduction

Rock is the most extensive geological material in nature. Stead and Wolter (2015) pointed out there were a large number of rock fault structures in the stratum, and their fault failures are directly related to geological disasters such as earthquakes, landslides and ground fissures, the same conclusions were drawn by Upton *et al*. (2018). With the increasing demand for various resources and energy, rock engineering activities such as deep mining engineering, water conservancy and hydropower Engineering and underground space excavation are increasing. These projects are related to rock fracture failure. The joints and cracks in rock expand under the external action and eventually lead to rock failure, and the expansion process follows the fracture mechanicstheory.

Rock fracture mechanics is an interdisciplinary subject of fracture mechanics, geophysics and geotechnical engineering. In the research method of rock fracture mechanics, the stress intensity factor is used to calculate the fracture toughness of rock, track the expansion of structural plane and evaluate the stability of engineering rock mass. Bouare *et al*. (2022) pointed out obtaining the high precision displacement field and stress intensity factor of sample are two of the key problems of rock fracture mechanics research and application. A novel J-integral method was coded by Miao *et al*. (2022) and adopted to quantify the SIF at the crack tip which inherently takes the FPZ into account. Zhang *et al*. (2022) used crack propagation gauges to measure crack propagation speed dynamic stress intensity factor. He and Shi (2019) studied the fracture performance of brittle materials using strain gauge. Digital image correlation (DIC) method was adopted to analysis the deformation field of brittle materials by Zhao *et al*. (2020). 2D-DIC has been analyzed to evaluate the influence of crack shielding during fatigue experiments conducted on two aluminium alloys tested at different stress ratios. (Diaz *et al*. 2020). Compared with the traditional strain measurement methods, DIC method has many advantages in analyzing the displacement field near the notch: full field measurement, non-contact and automation, *et al.*

There are many calculation methods to calculate stress intensity factor. For the convenience of querying, the empirical formulas were included in the book (Tada *et al.* 2000). Dimensionless stress intensity factors and T-stresses were calculated by using the finite element method for various crack lengths, crack angles and span to length ratios (Li *et al.* 2020). Stress intensity factor of an aero-engine compressor blade with crack was calculated by finite element method (Li *et al.* 2020). A series of three-point bending tests were performed and the DIC method was used to measure the full-field displacements of the specimens (Ji *et al.* 2016). Mokhtarishirazabad *et al.* (2020) presented a methodology based on a combination of digital image correlation and an analytical elastic solution to monitor the full-field displacement around a crack tip at different load levels. The application of weight function method in fracture mechanics was summarized by Wu *et al.* (2019). Seifi (2015) studied the stress intensity factors for internal surface cracks in autofrettaged functionally graded cylinders using weight function method. A general weight function was derived to evaluate the thermal stress intensity factors of a circumferential crack in cylinders by Nabavi and Ghajar (2010). However, manual contains limited forms

*Corresponding author, Assistant Professor
E-mail: caoshuwen@xauat.edu.cn
[a]Ph.D. Student

ISSN: 2005-307X (Print), 2092-6219 (Online)

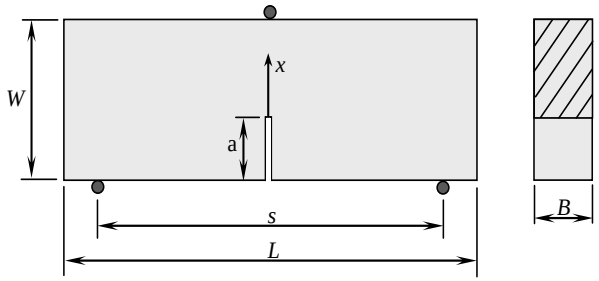

Fig. 1 Three-point bending testing specimen

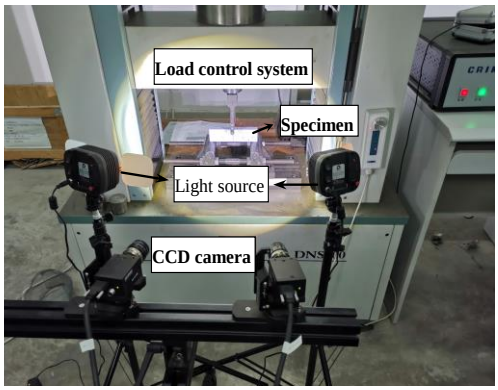

Fig. 2 Loading and acquisition system for three-point bending test

Table 1 Specimens size

α	Number	L/mm	W/mm	B/mm
0.1	0.1-1	161.1	41.36	21.12
	0.1-2	161.4	41.62	21.11
	0.1-3	161.1	41.22	20.74
0.2	0.2-1	161.2	41.56	21.21
	0.2-2	161.2	41.45	20.54
	0.2-3	161.6	41.34	21.40
0.3	0.3-1	161.5	41.34	21.38
	0.3-2	161.5	41.08	21.55
	0.3-3	161.6	41.68	21.58
0.4	0.4-1	161.7	41.12	20.94
	0.4-2	161.4	41.74	21.40
	0.4-3	161.3	41.25	21.06

of crack only. Finite element analysis method and optical test analysis method need a lot of time and specimens. The weight function method can be used to solve the stress intensity factor of cracks under arbitrary load conditions. It has the advantages of high precision, good efficiency and strong applicability. It has become an efficient method to calculate the stress intensity factor of cracks and has been widely used.

In this paper, the fracture tests of granite rectangular section specimens with type I precast notch under three-point bending loading were carried out. DIC method was used to analyze the evolution of crack tip opening displacement (CTOD) and horizontal displacement field of precast notch specimens with different depths; The stress intensity factors of granite specimens with precast cracks were derived by the weight functions method. The accuracy and applicability of the weight function method was verified by comparing different calculation methods.

2. Materials and methods

To analyze the influence of precast notch depth on fracture performance, four kinds of single notch granite three-point bending specimens with different precast notch depths were processed (Fig. 1), the specimen was processed as a cuboid with central precast notch, a is the precast notch depth, α(α= a/W) is the dimensionless notch depth. The effective span of the test piece S = 120 mm, and the size of the specimens are shown in Table 1.

The test system consists of loading system and digital image acquisition system (Fig. 2). The loading system is a DNS100 electronic universal testing machine, the speed control mode is adopted, and the loading rate is 0.02mm/min. The digital image acquisition system is the VIC-3D non-contact strain measurement system produced by CSI. Two CCD cameras with effective pixel of 2448 × 2048 were used as image acquisition device. The image acquisition rate is 1 frame/s for the first 4 minutes and 10 frame/s for the subsequent time. In the process of speckle production, matte white paint is used to make the bottom and matte black paint is used to make the speckle on the surface of the test specimens. The DIC software evaluation ensures that the resolution confidence reaches 0.01 pixels.

DIC is a non-contact, full field optical measurement technique capable of measuring both deformation and strain. DIC tracks the movement of multiple points during deformation, with correlation functions used to assess the similarity between regions of points. Two of these correlation functions are the Cross-Correlation function and Normalized Correlation Function, shown in Eqs. (1) and (2), respectively.

$$C(u,v)=\sum_{x=-n}^{n}\sum_{x=-n}^{n}I_1(x,y)I_2(x+u,y+v) \tag{1}$$

$$C'(u,v)=\frac{\sum_{x=-n}^{n}\sum_{x=-n}^{n}I_1(x,y)I_2(x+u,y+v)}{\sqrt{\sum_{x=-n}^{n}\sum_{x=-n}^{n}I_1^2(x,y)}\sqrt{\sum_{x=-n}^{n}\sum_{x=-n}^{n}I_1^2(x+u,y+v)}} \tag{2}$$

where I represents the image intensity, u and v represent changes in position in the x and y-direction.

3. Test results and analysis

3.1 Analysis of CTOD

CTOD can be used to indicate the fracture resistance of the specimen. Tests on three-point bending beams with different thicknesses show that CTOD has no size effect and

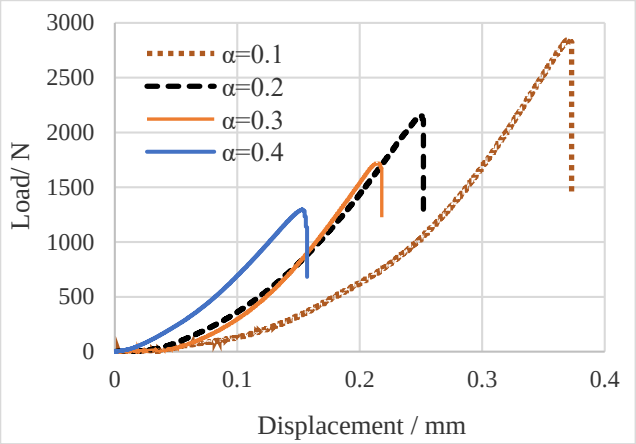

Fig. 3 Load displacement curves of specimens with different precast notch depths

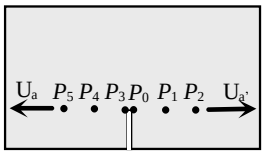

Fig. 4 Distribution of CTOD data points

is independent of specimen size. DIC method can analyze the CTOD changes of three-point bending beams with unilateral cracks conveniently.

Typical load displacement curves of specimens with different precast notch depths are shown in Fig. 3. The granite specimen has no obvious yield when it is destroyed, and the load drops at the moment of destruction suddenly, which is a typical brittle failure. The peak load and displacement decrease with the increase of precast notch depth α gradually. When the precast notch depth α changing from 0.1 to 0.4, the peak load decreases from 2853N to 1296N, 54.6%, reduced by 54.6%; The peak displacement reduced by 57.9% from 0.373 mm to 0.157 mm. With the increase of the depth of the precast notch, the effective height and the bearing capacity of the specimen decrease gradually.

It can be seen from Fig. 3 that the failure of granite is brittle fracture, therefore, three data points are symmetrically taken on both sides of the precast notch, and these points are distributed in the direction perpendicular to the notch (Fig. 4). P_0 and P_3 are distributed on both sides of the precast notch tip. In addition to P_0 and P_3, the distance between two adjacent data points is 0.5 mm. The CTOD of granite specimens can be calculated by Eq. (3)

$$\mathrm{CTOD} = U_{a'} - U_a \tag{3}$$

Where $U_{a'}$ is the average horizontal displacements of data points P_0, P_1 and P_2, U_a is the average horizontal displacements of data points P_3, P_4 and P_5. The horizontal displacements of each data point can be easily calculated by the displacement field value of DIC analysis.

One specimen was selected from each group, and the CTOD change curve of them was shown in Fig. 5. It can be seen that as a brittle material, granite has little change in the opening displacement of the crack tip at the initial time, and

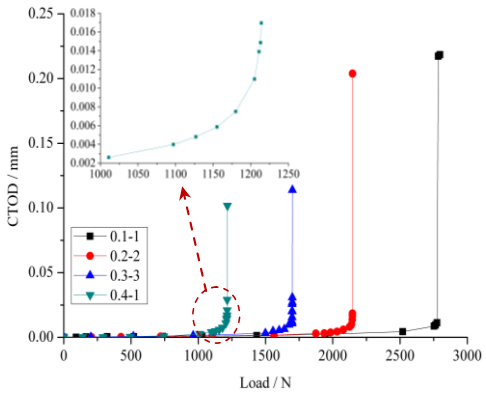

Fig. 5 CTOD curves of specimens with different precast notch depths

increases rapidly when approaching the critical load, which means that the specimen is fractured at this moment. With the increase of the precast notch length of granite specimen, the effective height of the beam decreases, the critical load decreases, and the corresponding CTOD value also decreases.

It can be seen from Fig. 5 that there is a curve transition stage before the sudden increase of CTOD value, which reflects the development of rock fracture process. With the increase of load, micro-cracks begin to appear at the crack tip, with the increase of micro-crack density, the distance between them decreases, micro-cracks converge gradually, and the crack propagation scale gradually increases. When the load reaches the critical value, the micro-cracks interpenetrate and develop into macro-cracks and fracture occurs.

3.2 Analysis of horizontal displacement

In order to analyze the horizontal displacement field near the precast notch of granite specimens, the typical displacement nephograms of different stress stages are selected (Fig. 6).

The number in the upper left corner of the cloud image represents the order of picture shooting. The displacement contours in the cloud map show a series of different color bands, which representing different horizontal displacements. The ribbon indicates that its internal displacement is close to a certain value, but not the exact same value. It can be seen from the figure that the horizontal displacements on both sides of the notch are symmetrically distributed.

The area near the notch tip is selected as the analysis area, and the coordinate system is established in this area. The x-axis is defined along the center of the precast notch, the y-axis is defined horizontally to the right, and the coordinate origin is located at the tip of the precast notch. Three different sections x= 0 mm, x= 6 mm and x= 12 mm are selected in the region, and 21 marker points are symmetrically selected on each section for horizontal displacement analysis, with the spacing of 2 mm between every 2 adjacent marker points (Fig. 7).

For the specimen with the dimensionless precast notch depth α=0.1, Fig. 8 shows the horizontal displacement ($\triangle u$)

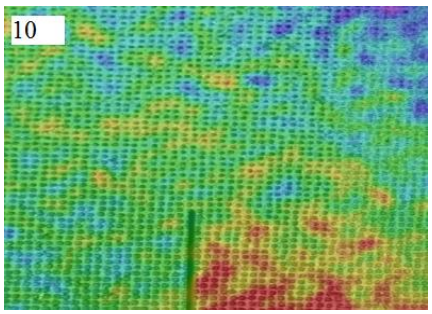

(a) horizontal displacement field of 10th photo

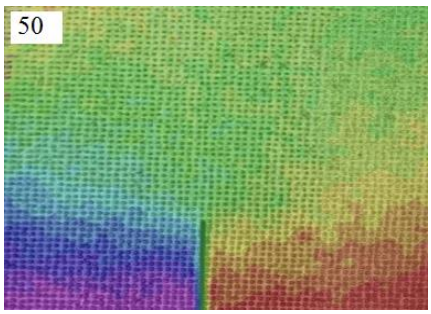

(b) horizontal displacement field of 50th photo

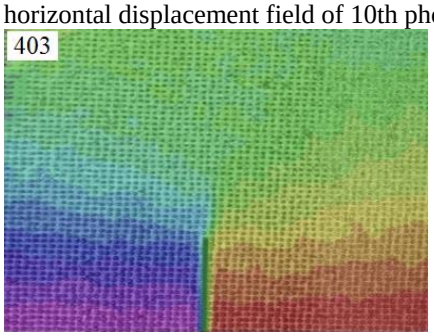

(c) horizontal displacement field of 403th photo

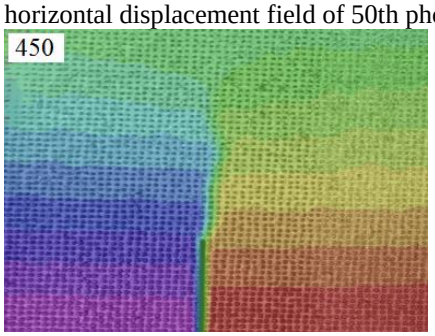

(d) horizontal displacement field of 450th photo

Fig. 6 Displacement field of crack tip under different loads

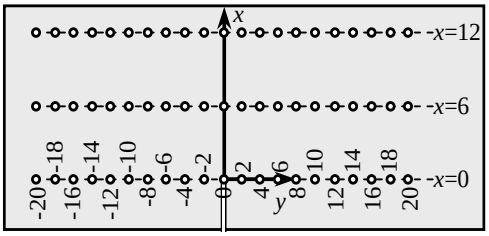

Fig. 7 Distribution of marker points

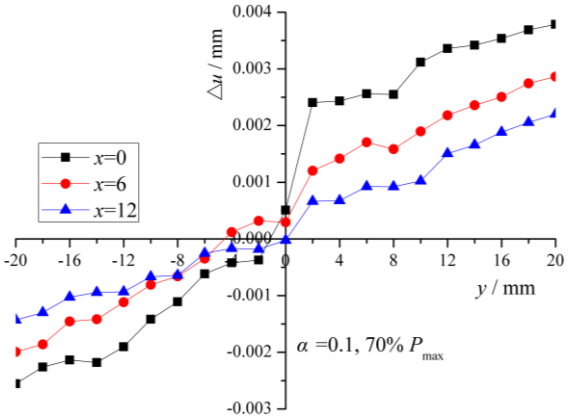

Fig. 8 Horizontal displacements distribution of specimen α=0.1 at different cross sections, 70% Pmax

distribution of the specimen surface along three different sections when the load reaches 70% of the maximum load P_{max}. For the specimen with α=0.1, the effective height of the specimen is H' =36 mm, and the distance between neutral axis and y-axis is 18 mm. The results show that the displacement decreases gradually with the section away from the y axis, such as x= 6 mm. If the cross section is close to the neutral axis, the displacement will be less and less, and eventually zero. Due to the symmetry of the specimen and the loading mechanism, the horizontal displacement along the loading center line is approximately zero. The displacements on both sides form a symmetrical pattern near the center line, and the slight asymmetry may be due to the misalignment of the specimen. At the precast notch tip section x=0, due to the stress concentration effect of the notch, there is a large horizontal displacement gradient in a small range (-2 mm <y < 2 mm) near the notch tip. At the x= 6 mm and x= 12 mm sections above the notch tip, the surface displacement of the specimen is approximately distributed as an elastic deformation law, and there is an approximately constant horizontal displacement gradient. The fluctuation of horizontal displacement value in the diagram may be caused by calculation error, specimen defects or imperfect specimen preparation.

With the increase of load, the notch tip begins to break and the displacement changes abruptly. Fig. 9 shows that when the load reaches 90% of the maximum load P_{max}, the horizontal displacement distribution of the specimen surface along different sections of the specimen α=0.1. From the horizontal displacement values of three different sections, the values at y= 0 are approximately zero. The values of other marker points at the cross section x = 0 and x = 6 mm are close to 0.01 mm and 0.007 mm respectively, indicating that the fracture process zone starting from the notch has developed to the cross section x = 6 mm above the notch tip, and the stress has been released. At the section x= 12 mm, the value at y= 4 mm is about 1.5 times that at y= 2 mm, which means that the macro crack has not yet developed to the section, but the micro crack has developed to the section.

For the specimen with the dimensionless precast notch depth α=0.4, Fig. 10 shows the horizontal displacement distribution of the specimen surface along three different

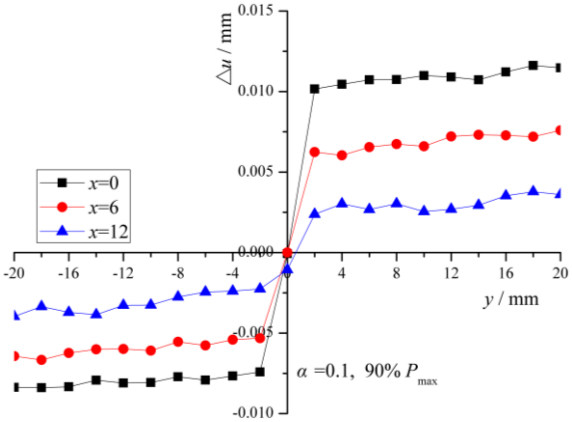

Fig. 9 Horizontal displacements distribution of specimen α=0.1 at different cross sections, 90% P_{max}

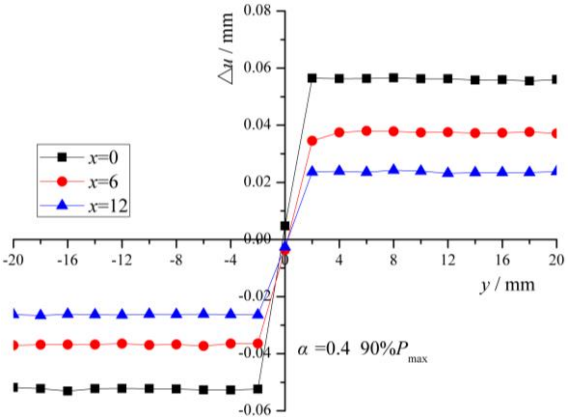

Fig. 11 Horizontal displacements distribution of specimen α=0.4 at different cross sections, 90% P_{max}

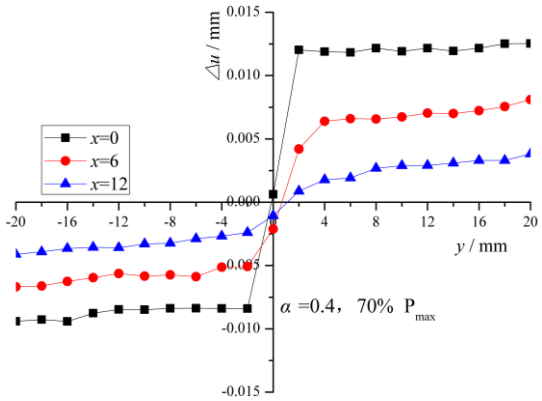

Fig. 10 Horizontal displacements distribution of specimen α=0.4 at different cross sections, 70% P_{max}

sections when the load reaches 70% of the maximum load P_{max}. Comparing Fig. 8, it can be seen that, similar to the specimen with α=0.1, there is a large horizontal displacement gradient in a small range (-2 mm < y <2 mm) near the notch tip at x = 0 due to the effect of stress concentration. However, the horizontal displacement of the other points at x=0 is approximately a fixed value, indicating that the precast notch tip has broken. It can be seen from the value at the cross section x = 6 mm that because the specimen has been fractured, the stress concentration at the tip of the fracture process zone leads to a large horizontal displacement gradient in a small range (-2 mm < y <2 mm). The value at y = 4mm is about 1.5 times that at y = 2 mm, indicating that the fracture has not yet developed to the cross section x = 6 mm. But the horizontal displacement of other points changes slowly, and the gradient is much smaller than that of the specimen with α = 0.1. At the section x= 12 mm, the surface displacement of the specimen is similar to that of the specimen with α = 0.1, which is approximately distributed in the law of elastic deformation, indicating that the crack has not yet developed to the upper section of the precast notch tip x = 12 mm.

Fig. 11 shows the displacement distribution of the dimensionless precast notch depth α=0.4 specimen when the load reaches 90% of the maximum load P_{max}. It can be seen from Fig. 9 that the values at x = 0 and x = 6 mm are similar to those of the specimen with α = 0.1. There is a large horizontal displacement gradient in the small range of -2 mm < y < 2 mm, and the horizontal displacement of other points are approximately a fixed value, which indicates that the macroscopic crack of the specimen has developed to the section x = 6 mm above the notch. At the section x = 12 mm, the surface displacement value is quite different from that of the specimen with α= 0.1. At this time, the horizontal displacement variation law of the section is similar to that of the section x = 0 and x = 6 mm, which is approximately a fixed value. This indicates that the macro crack has developed to x= 12 mm above the precast notch tip. It also reflects that with the increase of notch depth, the effective height of the specimen decreases, the bearing capacity decreases, and the specimen is more easily destroyed.

3.3 The stress intensity factor analysis

3.3.1 Weight function theory

According to the weight function theory of fracture mechanics, the stress intensity factor K can be obtained by integrating the product of the weight function m(a, x) and the stress distribution $\sigma(x)$ at the imaginary crack (Wu *et al*. 2019)

$$K = \int_0^a \sigma(x) \cdot m(\mathrm{a}, x)\mathrm{d}x \tag{4}$$

Where a is the precast notch length, x is the coordinate along the crack direction. Weight function m(a, x) is related to crack geometry (including load-displacement boundary conditions) only.

The precast notch of the three-point bending specimen belongs to the edge crack. For the convenience of derivation, the coordinate origin is located at the crack tip, and the coordinate axis is along the crack direction. The dimensionless parameters are introduced: α= a / W, ξ=x/ W, $\sigma(\xi)$/ σ_0. Where σ_0 is nominal stress. Eq. (4) can be rewritten as

$$K = f\sigma_0\sqrt{\pi \mathrm{a}} \qquad f = \int_0^{\mathrm{a}} \frac{\sigma(\xi)}{\sigma_0} \cdot \frac{m(\alpha, \xi/\alpha)}{\sqrt{\pi \mathrm{a}}}\mathrm{d}\xi \tag{5}$$

The analytic weight function m(a, x) is as follows (Wu *et al*. 2019)

$$m(\alpha,\xi/\alpha)=\frac{1}{\sqrt{2\pi a}}\sum_{i=1}^{5}\beta_i(\alpha)\cdot(1-\xi/\alpha)^{i-3/2} \tag{6a}$$

where

$$\beta_i(\alpha)=\frac{\left\{\alpha\cdot\frac{dF_{i-1}(\alpha)}{d\alpha}+\frac{1}{2}\left[(2i-1)\cdot F_i(\alpha)-(2i-5)\cdot F_{i-1}(\alpha)\right]\right\}}{f_r(\alpha)} \tag{6b}$$

$$i=1\sim 5$$

Where $F_i(\alpha)$ can be determined by normalized analytic weight function method(Wu *et al*. 2019), the value is determined by the known solution of stress intensity factor of edge crack of rectangular plate with finite width under a reference load.

The stress intensity factor under arbitrary $\sigma(x)$ can be obtained by integrating the product of analytic weight function $m(\alpha, \xi/\alpha)$ of edge crack and stress distribution $\sigma(x)$ of crack-free body at the hypothetical crack position according to Eq. (5). In practice, complex $\sigma(x)$ distributions are usually expressed by polynomials, each of which can be expressed as a power function distribution stress (Fig. 12)

$$\sigma(\xi)/\sigma_0=\xi^n \qquad 0\le\xi\le\alpha \tag{7}$$

Substituting Eqs. (6) and (7) into Eq. (5), the closed solution of dimensionless stress intensity factor f_n in the case of power function distribution stress can be obtained

$$\begin{aligned} f_n&=\int_0^a \xi^n\frac{m(\alpha,\xi)}{\sqrt{\pi a}}d\xi \\ &=\frac{2^{n+(1/2)}n!\alpha^n}{\pi}\cdot\sum_{i=1}^{5}\left[\beta_i(\alpha)\prod_{k=0}^{n}\frac{1}{2i-1+2k}\right] \end{aligned} \tag{8}$$

As shown in Table 2, the non-dimension stress intensity factor f_n of a single edge crack in a finite rectangular plate subjected to a power function distributed stress is obtained.

When the crack surface is subjected to polynomial distribution stress

$$\sigma(\xi)/\sigma_0=\sum c_n\xi^n \qquad 0\le\xi\le\alpha \tag{9}$$

The corresponding non-dimension stress intensity factor can be obtained by simple operations only

$$f=\sum c_n f_n \tag{10}$$

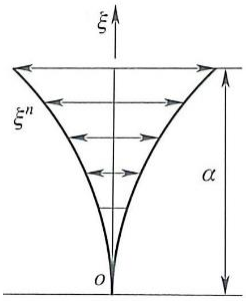

Fig. 12 crack line power stress loading

Table 2 Non-dimensional SIF f_n of finite rectangular plate under crack line power stress loading

α	n=0	n=1	n=2	n=3
0.1	1.1890	7.0886×10^{-2}	5.3977×10^{-3}	4.5017×10^{-4}
0.2	1.3672	1.5577×10^{-1}	2.3174×10^{-2}	3.8112×10^{-3}
0.3	1.6602	2.6753×10^{-1}	5.7829×10^{-2}	1.3985×10^{-2}
0.4	2.1113	4.2491×10^{-1}	1.1788×10^{-1}	3.7080×10^{-2}

The weight function method is used to calculate the stress intensity factor. In addition to the weight function $m(\alpha, \xi/\alpha)$ of the crack geometry, the non-dimension stress distribution $\sigma(\xi)/\sigma_0$ at the hypothetical crack in the crack-free body is also required. For the crack-free stress of any span-width ratio S/W three-point bending beam, Filon (1903) gave the classical analytical solution

$$\frac{\sigma(\xi)}{\sigma_0}=\frac{2\xi-1}{2}-\frac{8}{3(S/W)^2}(A_1+A_2+A_3+A_4) \qquad \sigma_0=\frac{3PS/W}{2WB} \tag{11a}$$

$$A_1=\sum_{n=1}^{\infty}\frac{\sinh(mW/2)-mW/2\cosh(mW/2)}{mW+\sinh(mW)}\cosh(my) \tag{11b}$$

$$A_2=\sum_{n=1}^{\infty}\frac{my\sinh(mW/2)}{mW+\sinh(mW)}\sinh(my) \tag{11c}$$

$$A_3=\sum_{n=1}^{\infty}\frac{\cosh(MW/2)-MW/2\sinh(MW/2)}{\sinh(MW)-MW}\sinh(My) \tag{11d}$$

$$A_4=\sum_{n=1}^{\infty}\frac{My\cosh(MW/2)}{\sinh(MW)-MW}\cosh(My) \tag{11e}$$

Where $m=4n\pi/S$, $M=(4n+2)\pi/S$, $y=(2\xi-1)W/2$.

The choice of the number of series expansion terms n in Eqs. (11(a))-(11(e)) depends on the accuracy of the solution. After the convergence analysis, when n = 100 and n = 125, the difference between the results is within 0.15%, so n= 100 is taken for this calculation. As shown in Fig. 13, taking S/W= 2, 4, 6, 8 and 10 as examples, the stress distribution $\sigma(\xi)/\sigma_0$ at the hypothetical crack is calculated according to Eqs. (11(a))- (11(e)).

Fitting the stress distribution at the hypothetical crack in polynomial power function form

$$\sigma(\xi)/\sigma_0=\sum_{n=0}^{3}C_n\xi^n \qquad \sigma_0=\frac{3PS/W}{2WB} \qquad 0\le\xi\le0.95 \tag{12}$$

The coefficients C_n in Eq. (12) are shown in Table 3.

The non-dimension stress intensity factors of three-point bending specimens with different S/W are obtained by summing the polynomial coefficients of the quasi-synthetic power function in Table 3 and the non-dimension strength factors in Table 2 according to Eq. (10). The final results are shown in Table 4.

Table 3 Crack line stress polynomial coefficients C_n for three point bending in Eq. (12)

C_n	S/W								
	2	3	4	5	6	7	8	9	10
0	0.9300	0.9376	0.9531	0.9627	0.9689	0.9734	0.9767	0.9792	0.9813
1	-2.6092	-2.3210	-2.2423	-2.1953	-2.1630	-2.1397	-2.1220	-2.1083	-2.0973
2	2.4218	1.5643	1.1831	0.9490	0.7913	0.6781	0.5929	0.5266	0.4735
3	-1.3050	-0.9130	-0.6946	-0.5570	-0.4643	-0.3979	-0.3479	-0.3089	-0.2777

Table 4 Non-dimensional SIF $f(a)$ of different precast notch

α	S/W								
	2	3	4	5	6	7	8	9	10
0	0.9125	0.9398	0.9624	0.9764	0.9855	0.9921	0.9970	1.0008	1.0038
1	0.9162	0.9531	0.9785	0.9941	1.0043	1.0117	1.0172	1.0214	1.0249
2	0.9677	1.0133	1.0411	1.0580	1.0692	1.0772	1.0832	1.0878	1.0916
3	1.0919	1.1438	1.1731	1.1909	1.2027	1.2111	1.2174	1.2223	1.2262

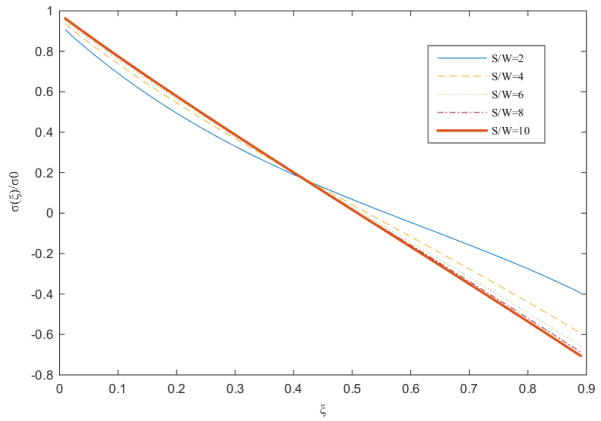

Fig. 13 Un-crack stress distribution for three-point bending beam of different span to width S/W (n=100)

3.3.2 The stress intensity factor of granite with different crack depths

Using the non-dimension stress intensity factor obtained in Table 4, combined with the measured rock specimen parameters such as specimen height, thickness and prefabricated crack depth, etc. the dimensional stress intensity factor can be obtained by the Eq. (13), and the results are shown in Table 5.

$$K = f\sigma_0\sqrt{\pi a} \qquad \sigma_0 = \frac{3PS/W}{2WB} \tag{13}$$

As shown in Table 5, the results are compared with Eqs. (12) and (13) (Tada *et al*. 2000).

$$K_{IC} = \frac{PS}{W^{1.5}B}F_1(a/W) \tag{14}$$

Where $F_1(a/W)=2.9(a/W)^{0.5}-4.6(a/W)^{1.5}+21.8(a/W)^{2.5}-37.6(a/W)^{3.5}+38.7(a/W)^{4.5}$

$$K_{IC} = \frac{3PS}{2W^2B}\sqrt{a}F_2(a/W) \tag{15}$$

Where

$$F_2(a/W) = \frac{1.99-(a/W)(1-a/W)\left[2.15-3.93a/W+2.7(a/W)^2\right]}{(1+2a/W)(1-a/W)^{3/2}}.$$

In the Eqs. (13)-(15), P is the applied load, S is the span of the specimen, W is the height of the specimen, B is the thickness of the specimen, a is the prefabricated crack depth.

From Table 5, it can be seen that the average stress intensity factor errors of each crack depth are no more than 1.5% compared with the calculation results of Eq. (14); Compared with the calculation results of Eq. (15), the average errors of stress intensity factor for each crack depth are no more than 3.5%. And the maximum error on the prefabricated crack α= 0.1. For other crack depth specimens, the average errors of stress intensity factor of each crack depth are not exceed 0.5%. Thus, it can be seen that the stress intensity factor of granite specimens deduced by the weight function method has sufficient accuracy when α=0.2~0.4, more data can be get by changing some parameters in Eq. (13), and experimental specimens and time are saved.

4. Conclusions

To study the mechanical performance of granite, experimental and theoretical studies are employed to explore the properties of the granite specimens with central notch. Based on test results and analysis of this paper, the following conclusions are drawn:

- With the increase of the precast notch depth, the effective height of specimen decreases, the critical load and the corresponding CTOD values decrease too.
- The horizontal displacement is distributed elastically as a whole, and it is layered from the displacement nephograms. Due to the stress concentration effect of the notch attachment, different horizontal displacement gradients are generated in a small range of -2 mm <y<2 mm for specimens with different notch depths. The crack

development height can be approximately analyzed by the gradient change of the horizontal displacement value of the same section marker point.

• Using the Wu-Carlsson analytical weight function of the edge crack of finite width plate, combined with the Filon analytical solution of the crack free stress distribution, according to the polynomial coefficient of the crack free stress distribution of three-point bending beam and the closed solution of the weight function under the power function stress, the stress intensity factor of three-point bending beam with span width ratio S/W=2~10 are obtained through simple operations. Compared with the existing method, the weight function method has the advantages of small error, high accuracy and time saving.

• For the weight function method, when the factors affecting the stress intensity factor (load and crack size) change, only the changed parameters need to be substituted into the stress intensity factor expression, and the value of the stress intensity factor at the crack tip can be quickly solved.

Acknowledgments

The research described in this paper was financially supported by the Special Fund of Shaanxi Education Department (Grant No.20JK0711), which were highly appreciated by the authors.

References

Bouare, H., Mesgouez, A. and Lefeuve–Mesgouez, G. (2022), "Stress and displacement fields around an arbitrary shape tunnel surrounded by a multilayered elastic medium subjected to harmonic waves under plane strain conditions", *Soil Dynam. Earthq. Eng.*, **154**, 107158. https://doi.org/10.1016/j.soildyn.2022.107158.

Diaz, F.A., Vasco-Olmo, J.M., Lopez-Alba, E., Felipe-Sesé, L., Molina-Viedma, A.J. and Nowell, D. (2020), "Experimental evaluation of effective stress intensity factor using thermoelastic stress analysis and digital image correlation", *Int. J. Fatigue*, **135**, 105567. https://doi.org/10.1016/j.ijfatigue.2020.105567.

Filon L.N.G. (1903), "On an approximate solution for the bending of a beam of rectangular cross-section under any system of load, with special reference to points of concentrated or discontinuous loading", *P. Roy. Soc. London*, **201**, 63-155. https://doi.org/10.1098/rsta.1903.0014.

He, J.J. and Shi, J.P. (2019) "Experimental study on three-point bending fracture performance and failure morphology of basalt under different loading rates", *Exp. Mech.*, **34**(4), 666-674. (in Chinese). https://doi.org/10.7520/1001-4888-18-005.

Ji, W., Pan, Z., Miao, S., *et al.* (2016), "Fracture characteristics of two type of rock based on digital image correlation", *Chinese J. Rock Soil Mech.*, **37**(8), 2299-2305. (in Chinese). https://doi.org/10.16285/j.rsm.2016.08.023.

Li, Y., Dong, S. and Pavier, M.J. (2020), "Measurement of the mixed mode fracture strength of green sandstone using three-point bending specimens", *Geomech. Eng.*, **20**(1), 9-18. https://doi.org/10.12989/gae.2020.20.1.009.

Li, C., Luo, X., Yang, B., *et al.* (2013), "Stress intensity factor calculation for aero-engine compressor blade with finite element method", *Chinese J. Appl. Mech.*, **30**(3), 373-377. (in Chinese). https://doi.org/10.11776/cjam.30.03.B069.

Miao, S., Pan, P.Z., Hou, W., He, B. and Yu, P. (2022), "Stress intensity factor evolution considering fracture process zone development of granite under monotonic and stepwise cyclic loading", *Eng. Fract. Mech.*, **273**, 108727. https://doi.org/10.1016/j.engfracmech.2022.108727.

Mokhtarishirazabad, M., Lopez-Crespo, P. and Zanganeh, M. (2018), "Stress intensity factor monitoring under cyclic loading by digital image correlation", *Fatigue Fract. Eng. Mater. Struct.*, **5**, 1-10. https://doi.org/10.1111/ffe.12825.

Nabavi, S.M. and Ghajar, R. (2010), "Analysis of thermal stress intensity factors for cracked cylinders using weight function method", *Int. J. Eng. Sci.*, **48**(12), 1811-1823. https://doi.org/10.1016/j.ijengsci.2010.08.006.

Seifi, R. (2015), "Stress intensity factors for internal surface cracks in autofrettaged functionally graded thick cylinders using weight function method", *Theor. Appl. Fract. Mech.*, **75**, 113-123. https://doi.org/10.1016/j.tafmec.2014.11.004.

Stead, D. and Wolter, A. (2015). "A critical review of rock slope failure mechanisms: the importance of structural geology", *J. Struct. Geol.*, **74**, 1-23. https://doi.org/10.1016/j.jsg.2015.02.002.

Tada, H., Paris, P.C. and Irwin, G.R. (2000), *The Stress Analysis of cracks handbook*, ASME Press, New York, USA.

Upton, P., Koons, P.O. and Roy, S.G. (2018). "Rock failure and erosion of a fault damage zone as a function of rock properties: Alpine Fault at Waikukupa River", *New Zealand J. Geol. Geophys.*, **61**(3), 367-375. https://doi.org/10.1080/00288306.2018.1430592.

Wu, X.R., Tong, D. and Wu, X., *et al.* (2019), *Weight function methods in fracture mechanics*: *Theory and applications*, Aviation Industry Press, Beijing, China. (in Chinese).

Zhang, X., Ma, L., Zhu, Z., Zhou, L. and Wang, M. (2022), "Experimental study on the energy evolution law during crack propagation of cracked rock mass under impact loads", *Theor. Appl. Fract. Mech.*, **122**, 103579. https://doi.org/10.1016/j.tafmec.2022.103579.

Zhao, T., Zhang, W., Gu, S., Lv, Y. and Li, Z. (2020), "Study on fracture mechanics of granite based on digital speckle correlation method", *Int. J. Solids Struct.*, **193**, 192-199. https://doi.org/10.1016/j.ijsolstr.2020.02.026.

IC